Published in final edited form as:
Neuroimage. 2013 January 15; 65: 209–215. doi:10.1016/j.neuroimage.2012.10.021.

White-Matter Diffusion fMRI of Mouse Optic Nerve

William M. Spees[a,b], **Tsen-Hsuan Lin**[a], and **Sheng-Kwei Song**[a,b]

[a]Biomedical MR Laboratory, Department of Radiology, Washington University School of Medicine, St. Louis, MO USA

[b]Hope Center for Neurological Disorders, Washington University School of Medicine, St. Louis, MO USA

Abstract

Non-invasive assessment of white-matter functionality in the nervous system would be a valuable basic neuroscience and clinical diagnostic tool. Using standard MRI techniques, a visual-stimulus-induced 27% decrease in the apparent diffusion coefficient of water perpendicular to the axonal fibers ($ADC_{\perp}$) is demonstrated for C57BL/6 mouse optic nerve *in vivo*. No change in $ADC_{||}$ (diffusion parallel to the optic nerve fibers) was observed during visual stimulation. The stimulus-induced changes are completely reversible. A possible vascular contribution was sought by carrying out the $ADC_{\perp}$ measurements in hypercapnic mice with and without visual stimulus. Similar effects were seen in room-air-breathing and hypercapnic animals. The *in vivo* stimulus-induced $ADC_{\perp}$ decreases are roughly similar to literature reports for *ex vivo* rat optic nerve preparations under conditions of osmotic swelling. The experimental results strongly suggest that osmotic after-effects of nerve impulses through the axonal fibers are responsible for the observed ADC decrease.

Keywords

Diffusion; White Matter; Optic Nerve; fMRI; Mouse

Introduction

Currently functional MRI (fMRI) studies are limited almost exclusively to gray matter, and rely upon coupling of hemodynamic response to functional activation (Logothetis, 2008). Signal modulations on the order of 1 – 5% are typical. The limited capacity for physiologic modulation of blood flow and the inherently lower fractional blood volume probably account for the difficulty in monitoring white-matter functional activation with standard BOLD (Blood Oxygen Level Dependent) fMRI techniques (Gawryluk et al., 2009; Rostrup et al., 2000). Thus, at present, white-matter MRI is largely restricted to probing the structural integrity of fiber tracts using diffusion tensor imaging or variants thereof (Jones, 2010).

Corresponding Author: William M. Spees, Ph.D. Biomedical MR Laboratory, Department of Radiology, Campus Box 8227, Washington University School of Medicine, 660 South Euclid, St. Louis, MO 63110, phone: 314-747-1373, fax: 314-362-0526, spees@wustl.edu.

Diffusion weighting has been investigated as a potential alternative to BOLD for monitoring neuronal activity in gray matter of the human visual cortex (Le Bihan et al., 2006). An ~1 – 2% increase in diffusion weighted MRI signal intensity was reported ($b = 1.8$ ms/μm^2), suggested to arise from activity-dependent cell swelling. In a subsequent report, a similar diffusion-weighted MRI signal intensity increase was elicited via hypercapnia-induced brain blood flow enhancement without neuronal activation (Miller et al., 2007). Thus, the specificity of diffusion fMRI signal change to neuronal activity may be confounded by a sizeable vascular contribution.

In *ex vivo* rat optic nerve preparations, repeated electrical stimulation produces frequency- and duration-dependent shrinkage of the extracellular space (ECS), with higher frequencies and longer stimulus trains resulting in a more pronounced ECS reduction (Ransom et al., 1985). A consensus has emerged that the observed ECS shrinkage results from an osmotic shift of water into glial cells as part of a mechanism for maintaining extracellular ionic balance and neuronal electrophysiologic competence (Ransom and Sontheimer, 1992; Rash, 2010; Schwartzkroin et al., 1998; Sykova and Chvatal, 1993).

To determine the feasibility of detecting diffusion weighted MRI signal changes in white matter responding to functional stimulation, as well as the specificity of this signal change to axonal activation, optic nerves from room-air-breathing and hypercapnic mice were examined with and without the application of visual stimulus.

Materials and Methods

Animals

All experimental procedures were in compliance with the protocol approved by the Washington University Animal Studies Committee. Female C57BL/6 mice, aged 10 – 12 weeks, obtained from Jackson Laboratory (Bar Harbor, ME) were used in the experiments.

Visual Acuity

Prior to MRI experiments, visual acuity of each mouse was measured with a Virtual Optokinetic System (CerebralMechanics, Inc.) as previously reported (Prusky et al., 2004), to ensure normal vision.

Animal Monitoring

Respiratory rate and rectal temperature of anesthetized mice were monitored during experiments using an MR-compatible animal monitoring system (Small Animal Instruments, Inc., Stony Brook, NY) to ensure physiologic stability. A body-core temperature of 37°C was maintained via a circulating warm water pad placed underneath the animal and thermostated warm air blown into the magnet bore.

Anesthesia

The anesthesia regimen employed has been shown to maintain fMRI-observable neuronal response in mice (Adamczak et al., 2010). Anesthesia was induced with 2.5% isofluorane in O_2, and reduced to 1.5% for placement of the animal in the imaging cradle. After positioning of the animal in a head holder and achieving a stable respiratory rate, a subcutaneous 0.3 mg/kg bolus of medetomidine was administered. Beginning three minutes after the bolus injection, isofluorane levels were reduced by ~ 0.2% per minute until the inhaled gas consisted of 100% O_2. At 10 minutes after the bolus injection, continuous subcutaneous infusion of medetomidine was initiated at a rate of 0.6 mg/kg/hr, and the nose cone for inhalant anesthetics was removed, leaving the animal breathing room air for the duration of the MR experiment. In experiments investigating the effect of hypercapnia (air

vs. 5% CO_2/95% O_2), the animal, head holder, and other equipment was placed in a closed plastic tube that allowed control of the breathing gas composition.

Magnetic Resonance Imaging

MRI experiments were performed on a 4.7-T Agilent DirectDrive™ Small-Animal MRI system (Agilent Technologies, Santa Clara, CA), equipped with Magnex/Agilent HD imaging gradients (Magnex/Agilent, Oxford, UK). The gradient hardware, interfaced with a set of IEC 300 A gradient power amplifiers (International Electric Company, Helsinki, Finland), is capable of pulsed gradient strengths up to 58 G/cm with a gradient rise time ≤ 295 μs. An actively-decoupled volume (transmit)/surface (receive) coil pair was used for MR excitation and signal reception (Garbow et al., 2008). A diffusion-weighted, multi-echo spin-echo imaging sequence (Tu et al., 2010) was employed for scout images and also for the final targeted diffusion-weighted images (Fig. 1). To minimize partial volume effects in optic nerve diffusion measurements, the image plan was adjusted to ensure that, as nearly as possible, the optic nerve fibers were orthogonal to the image slice plane (Figs. 2b and 2c). Image acquisition parameters included a slice thickness of 1.3 mm and a 20 × 20 mm^2 (256 × 256) field-of-view. A sequence repetition time of 1.5 s was employed, thus the total acquisition time for a pair of diffusion-weighted images (low and high b values) probing a single diffusion direction was 12.8 minutes. To increase accumulated signal-to-noise ratio for each phase-encoding step, a train of three echoes were co-added to form the final MR images. The first echo time (which included a pair of diffusion-weighting gradient lobes centered about the 180° refocusing pulse) was 37.1 ms, with a spacing of 23.6 ms between the first and all subsequent echoes without diffusion gradients.

Some evidence for attenuated ADC response with repeated applications of visual stimulus after the initial “on” block was seen (data not shown). This could possibly result from accumulation of inactive forms of retinal rhodopsin during the rather lengthy 12.8-minute stimulus block (Lee et al., 2010). To avoid potentially confounding results, $ADC_{\perp}$ and $ADC_{\parallel}$ were measured in separate cohorts of animals.

For each experimental condition (e.g., baseline, visual “stimulus on”, post- “stimulus off”, etc.) a low and high b-value diffusion-weighted image was acquired from a single slice (Fig. 2c). For the cohort in which $ADC_{\perp}$ was evaluated, b values of 0.10 ms/μm^2 and 1.40 ms/μm^2 were used (δ = 5 ms, Δ = 18 ms, G_{diff} = 6 G/cm or 22.6 G/cm for a pair of trapezoidal diffusion-weighting gradients). Because of the much less restricted diffusion along the axis of the optic nerve (Fig. 3), measurements in the $ADC_{\parallel}$ cohort were made based on a pair of diffusion-weighted images having b values of 0.10 ms/μm^2 and 0.70 ms/μm^2 (δ and Δ were the same as for $ADC_{\perp}$ measurements, but G_{diff} = 6 G/cm or 15.5 G/cm). It is worth pointing out that, in the diffusion MR literature, b values reported in units of s/mm^2 are not uncommon, with ADC being reported in mm^2/s units in that case. To convert to those units, our numerical values for b should be multiplied by 1,000 and our ADC numbers divided by 1,000.

Visual Stimulation

Visual stimulation was achieved by repetitive flashing of a high-intensity, white LED (Cree, Model C503C-WAS) fixed at a position 5 cm in front of the animal’s nose and aimed at one of the animal’s eyes. Light was blocked out of the contralateral eye with two layers of black electrical tape. A step-function signal of 1.4 Hz frequency (Ridder III and Nusinowitz, 2006), 200 ms on/514 ms off, with amplitude of 4 V/0 V (on/off) was provided by a Grass Instruments S9 stimulator (Grass Technologies, West Warwick, RI). With a 100 Ω series current-limiting resistor, the forward voltage across the LED is 3.2V. The circuit draws 8 mA of DC current in the “on” state, corresponding to a luminous intensity of ~ 14 candela.

DC current was carried from the stimulator (outside the magnet) through the LED (inside the RF-shielded bore of the magnet) by a pair of coaxial BNC cables. Additionally, a pair of 3-segment LC filters was placed on each BNC line where it fed into the magnet bore to eliminate delivery of unwanted RF interference into the magnet. The outer conductor of each BNC line was grounded to the magnet's RF shield at the feedthrough into the magnet. In MRI measurements with "stimulus on", the flashing light stimulus was applied for the entire 12.8-minute duration of the imaging acquisition.

While white matter tends to be less well-vascularized than gray matter structures, the vascularization of the mouse optic nerve is not negligible, with retinal venous drainage routed within close proximity to the ROI investigated (May and Lutjen-Drecoll, 2002). In order to determine the effect of possible dilation of optic nerve vasculature and associated changes in blood oxygenation level on the observed $ADC_{\perp}$ decrease, "baseline" and "stimulus on" measurements were also made in anesthetized mice breathing a mixture of 5% CO_2/95% O_2 (n = 5). In cases where the breathing-gas composition was changed, a period of 5 minutes was allowed prior to the commencement of MR measurements.

ADC Maps

The signal intensity, S(b), in the range of b values employed for $ADC_{||}$ and $ADC_{\perp}$ estimation is essentially a monoexponential decay, although the signal-decay behavior for $ADC_{\perp}$, it should be noted, is more complex than this over a wider range of b values (Fig. 3). As is commonly done in measurements at only two b values, the following equation was employed to estimate both $ADC_{||}$ and $ADC_{\perp}$:

$$\ln\left[\frac{S(b')}{S(b)}\right] = -(b' - b)\cdot \mathrm{ADC}. \quad (1)$$

ADC maps were generated according to Equation 1 using the pair (high-b and low-b) of diffusion-weighted images.

Image Segmentation

For estimation of $ADC_{\perp}$, optic nerve ROIs were prescribed based upon the normalized diffusion-weighted (b = 1.40 ms/μm^2) image and the ADC map as described below.

First, the mean signal intensity was determined for a 20 voxel × 20 voxel region-of-interest drawn within the basal forebrain (a brain region not expected to be activated with visual stimulation, but loacated within a reasonable proximity to the optic nerve). The basal forebrain ROI's mean intensity was employed in the denominator to normalize the b = 1.4 ms/μm^2 diffusion-weighted images. In Figure 2c and 2d, it can be appreciated that the image acquired with diffusion-weighting perpendicular to the optic nerve fibers provides fairly clear definition of the optic nerve.

Two separate operators manually drew optic nerve ROIs on a set of five normalized diffusion-weighted images (b = 1.4 ms/μm^2). Based on statistical analyses (mean and standard deviation) of the resulting collection of normalized voxel intensities, a lower-bound normalized-intensity threshold was established (lower-limit intensity threshold = mean −2 × std). The first operator found a normalized lower-limit intensity threshold of 0.75 for the optic nerve. The second operator determined a threshold of 0.86. In general, signal intensity decreases and ADC increases at the periphery of the nerve in the diffusion-weighted images as the partial-volume contribution of surrounding CSF increases. The more stringent

normalized-signal-intensity cutoff of 0.86 was employed in all subsequent analyses as described further below.

After having established the normalized-signal-intensity threshold, we determined an ADC threshold for optic nerve voxels. On the same set of five images with a 512 × 512 image matrix, optic nerve ROIs were defined that were reduced by one voxel away from the edge of the 0.86 threshold on the normalized diffusion-weighted images. This was to further reduce partial-volume contributions. It was found that 95% of the resulting voxels had $ADC_{\perp} < 0.31\ \mu m^2/ms$. In general, more peripheral voxels had higher $ADC_{\perp}$, presumably as a result of increased CSF partial volume contributions. These results were used to establish image-intensity and ADC-based criteria for determining whether or not a given voxel was eligible for assignment to the optic nerve or not.

For routine analysis, the 512 × 512 diffusion-weighted image data and ADC maps were interpolated to a 1024 × 1024 matrix in ImageJ software (U.S. National Institute of Health, Bethesda, MD, http://imagej.nih.gov/ij/). On the diffusion-weighted ($b = 1.40\ ms/\mu m^2$) image, a mask was generated encompassing all contiguous optic nerve voxels with normalized signal intensity ≥ 0.86. On the $ADC_{\perp}$ map (constructed from the b = 0.1 and $b = 1.40\ ms/\mu m^2$ diffusion-weighted images according to Equation 1) a second mask was generated, encompassing contiguous voxels with $ADC_{\perp} < 0.31\ \mu m^2/ms$. As might be expected, the ADC and normalized intensity masks had a very high degree of overlap.

The following prescription was used for defining the final optic nerve regions-of-interest. The largest possible ROI was inscribed inside the normalized-signal-intensity and $ADC_{\perp}$ masks adhering strictly to the guidelines that: (i) an ROI voxel lie within both masked regions and (ii) that an ROI voxel could not touch the perimeter of the signal-intensity mask, but could touch the perimeter of the ADC mask. For determining ROI membership in cases of voxels on the periphery, wherein the definition of the ROI periphery (defined by conditions i and ii, above) did not co-register perfectly, the more interior (less peripheral) of the two boundaries was honored. This was favored in order to reduce the partial-volume contributions to the optic-nerve ROI measurements as much as possible. Individual ROIs ranged in size from 53–134 voxels from the 1024 × 1024 images ($20{,}000 – 51{,}000\ \mu m^2$).

The contrast in parallel-diffusion-weighted images does not readily reveal the definition of the optic nerve. For measurements of $ADC_{||}$, each pair of diffusion-weighted images was preceded and followed by a single diffusion-weighted image with diffusion gradients applied perpendicular to the nerve fibers and $b = 1.40\ ms/\mu m^2$. The definition of the ROI was then prescribed referencing the images acquired with perpendicular diffusion weighting.

Statistical Tests

Repeated-measures ANOVA was performed to assess for differences between group data using *Statistica* software (StatSoft, Tulsa, OK). Measurements on the contralateral and ipsilateral optic nerves under the various experimental conditions were treated as repeated intra-subject measurements. Statistically significant differences between repeated measurements (e.g., ipsilateral optic nerve: “baseline” vs. “stimulus on” vs. “stimulus off”, contralateral optic nerve: “baseline” vs. “stimulus on”, etc.) were identified via Fisher Least Significant Difference post-hoc testing.

Results

The imaging protocol employed provides good quality images of the mouse optic nerve. Signal-to-noise ratio varied across the study animals in the range from 22.3 to 30.3 with low

diffusion weighting (b = 0.1 ms/μm^2) and 17.2 to 25.1 for higher diffusion weightings (b = 1.4 ms/μm^2).

In the cohort of animals for which $ADC_{\perp}$ was measured (n = 5 mice), a sizeable and statistically significant 27% decrease (p = 0.0008, Baseline vs. Stimulus On) from 0.176 ± 0.019 μm^2/ms to 0.129 ± 0.013 μm^2/ms (mean ± sem, see Fig. 4 and Table 1) was observed. In individual animals, the range of $ADC_{\perp}$ decrease with stimulation was between 9% and 35%. The change was reversible with cessation of visual stimulation. In the contralateral control optic nerve, no systematic variation in $ADC_{\perp}$ was detectable with application of stimulus to the ipsilateral eye (Fig. 4). Additionally, the ADC measurements from within the reference basal forebrain region were quite stable with variations no more than 3% both intra- and inter-subject. From the inset in Figure 4, it can be appreciated that the inter-subject variation in $ADC_{\perp}$ is then largely a result of partial volume effects as the mouse optic nerve is surrounded by CSF which, by comparison, has a relatively high diffusivity.

No statistically significant effect in optic nerve $ADC_{||}$ was observed with the application of visual stimulation [$F(5,25) = 1.92$, $p = 0.13$, Fig. 5 and Table 1, n = 6 mice]. Again, ADC in the basal forebrain region was very stable across and within animals studied in this group.

Hypercapnia, by itself, produced no measureable changes in the optic nerve $ADC_{\perp}$ (Fig. 6 and Table 2, n = 5 mice). An activation-induced reversible 19% decrease in optic nerve $ADC_{\perp}$ (p = 0.008) was observed in hypercapnic mice, roughly similar to that seen in room-air-breathing animals. As can be appreciated from Figure 6, the measurements of $ADC_{\perp}$ in the cohort of animals in the hypercapnia experiments show more variability than that seen in the air-breathing stimulus experiments depicted in Figure 4, but not in any systematic way. This appears to be due to a variable shift in each animal's posture during carbogen exposure. During breathing of the 5% CO_2/95% O_2 gas mixture, the respiratory rate typically increased from ~ 130 breaths-per-minute to ~ 150 breaths-per-minute. In serial images of individual animals, the positions of some of the animals' optic nerves appear to shift by as much as 200 – 300 μm upon changing the composition of the gas mixture. Presumably this shift in position can be accompanied by loss of orthogonality between the optic nerve axis and the targeted image slice plane. Such a shift, of even a few degrees, can cause a variable partial volume contribution from the CSF that surrounds the mouse optic nerve. Systematic variations of similar magnitude in the measured $ADC_{\perp}$ can be produced by intentionally misaligning the slice plane by ~ 5° (data not shown). The stereotactic head holder provides a three-point restraint. If it were practical, implementation of a five-point head restraint might be capable of completely eliminating such small magnitude head motions.

Overall, the results of the hypercapnia + stimulation experiments strongly suggest that the observed decrease in optic nerve ADC with visual stimulation does not arise from a vascular effect (Miller et al., 2007) and is produced as a result of repeated axonal firing. The effect of hypercapnia and hypercapnia + stimulation on $ADC_{||}$ was not investigated.

Discussion

Our results show that *in vivo* diffusion MRI is capable of detecting the $ADC_{\perp}$ decrease (~27%) accompanying mouse optic nerve activation in medetomidine-anesthetized mice. The activation-associated $ADC_{\perp}$ decrease is independent of blood flow effects since hypercapnia alone does not produce observable changes, and a similar activation-induced decrement in $ADC_{\perp}$ was seen in hypercapnic and air-breathing mice. The extent of *in vivo* $ADC_{\perp}$ change is comparable to that reported (31 ± 8% decrease) for depolarization and osmotic swelling of *ex vivo* rat optic nerve at 21°C (Anderson, 1996) supporting the notion

that decreased ECS (Sen and Basser, 2005) may be responsible for the detected ADC change.

Decreased ADC is a hallmark of repeated, synchronous neuronal discharge in CNS. For example, 11 – 35% decreases in ADC were observed in 10 patients with complex partial status epilepticus (Szabo et al., 2005). Application of trains of electrical shocks, administered via carbon electrodes placed on the surface the rat brain, have been shown to result in an 8% decrease in gray-matter water ADC (Zhong et al., 1997). Spreading depression also produces a transient ADC drop (Latour et al., 1994; Sotak, 1999). While all of these conditions produce membrane depolarization and subsequent cellular swelling (Sotak, 1999), it is likely the cellular swelling aspect that is directly responsible for the observed changes in tissue water diffusion. For instance, membrane depolarization without cell swelling was not sufficient to produce changes in ADC in *ex vivo* rat optic nerve (Anderson, 1996).

In the current study, repetitive axonal firing within the optic nerve is expected to result from the flashing light stimulus. The frequency of 1.4 Hz for the repetitive light flashing was chosen since it is in the region of maximal response in the electroretinogram and visual evoked potential (voltage amplitude vs. flashing-stimulus frequency), as reported previously for measurements in C57BL/6 mice (Ridder III and Nusinowitz, 2006).

In the visual system, light intensity information is encoded by the excitation frequency of retinal ganglion cells (Hartline, 1934) with faithful transmission of the photoreceptor action potentials to the brain via the optic nerve. It is likely that during the 200ms-long pulses of bright light (repeated at 1.4 Hz temporal frequency), the mouse optic nerves are repetitively transmitting action potentials at frequencies of many tens of Hz (Nakamura et al., 2011; Rothe et al., 1999). *Ex vivo* rat optic nerves have been shown to undergo an ECS shrinkage that is more pronounced at higher rates of repeated electrical stimulation (Ransom et al., 1985). While it was not investigated here, we would expect that the ADC response in optic nerve should be graded in proportion to intensity of the applied stimulus. Earlier attempts to measure changes in $ADC_{\parallel}$ and $ADC_{\perp}$ in electrically-stimulated white matter of the *ex vivo* frog spinal cord were unsuccessful (Gulani et al., 1999), possibly due to the low-frequency (2.7 Hz average) of the applied electrical stimulus.

Taken together, our results for $ADC_{\perp}$ and $ADC_{\parallel}$ predict an enhanced relative anisotropy for activated white-matter fibers. Provided that stimulus paradigms can be devised for activating specific white-matter pathways (Gawryluk et al., 2009), it may be possible to monitor brain white-matter activation. A recent report was aimed at detecting white-matter diffusion anisotropy changes in humans with visual and tactile stimuli (Mandl et al., 2008). The conclusion reached in that study was that a large number of measurements would be required for reliable detection of diffusion MRI signal changes. This lack of sensitivity may reflect more on the need for higher spatial resolution (to avoid partial volume effects) than a lack of robust physiological response.

In the current study, we have used two diffusion-weighted measurements to estimate the ADC of optic nerve with and without visual stimulation, assuming diffusion-attenuated signal decays as a single exponential. As can readily be seen from Figure 3, this is approximately correct over the range of b values employed for estimation of $ADC_{\perp}$ and $ADC_{\parallel}$. Measurement with diffusion-weighting perpendicular to the optic nerve and b = 1.40 $ms/\mu m^2$ results in a relative signal intensity change of ~ 6.6% with vs. without stimulation.

Hypercapnia, a potent vasodilator and modulator of CNS blood flow (Rostrup et al., 2000), by itself did not elicit signal changes in the mouse optic nerve. A modulation in tissue ADC is one conceivable consequence of vasodilation (increased delivery of oxygenated blood)

with the same level of tissue oxygen consumption. The vascular network, especially the venous network, contains some amount of relatively paramagnetic deoxyhemoglobin. The confinement of this paramagnetic material to the venous network produces unintended tissue-internal magnetic field gradients (in addition to the intentionally-applied diffusion-weighting gradients). Reducing the tissue-internal field gradients, by reducing vascular deoxyhemoglobin content, can produce an increased tissue ADC (Does et al., 1999; Zhong et al., 1991). No such effects were observable in hypercapnic mice and essentially the same relative decrease in $ADC_{\perp}$ was seen with stimulation in hypercapnic and room-air-breathing animals.

We believe that ECS shrinkage in the optic nerve with visual stimulation is the cause of the observed ADC decrease. Interestingly, for both the rat optic nerve (Ransom et al., 1985) and rat spinal cord gray matter (Sykova and Chvatal, 1993), the extent of activity-dependent ECS shrinkage (from repeated electrical stimulation) is correlated with age of the animal. Both sets of authors noted that a key developmental feature in the maturation of these tissues is gliogenesis. Glial cells are often implicated as the dominant contributors to activity-induced ECS shrinkage in neural tissue (Ransom and Sontheimer, 1992; Schwartzkroin et al., 1998; Walz, 1989). As recently reviewed by Rash (Rash, 2010) the panglial syncytium (involving gap-junction-interconnected astrocytes, epindymocytes and oligodendrocytes--including direct involvement of myelin-bounded cytoplasmic spaces), is believed to provide a dynamic mechanism for potassium siphoning. This means of moving K^+ and osmotically accompanying water away from the axonal exterior is believed to allow for re-establishment of axonal membrane polarization required for the repeated propagation of action potentials.

It should be noted, that in addition to glial swelling, there is evidence for activity-dependent swelling of neuronal processes. Long-lasting swelling of dendritic spines has been reported following a 30-second period of *in vivo* electrical stimulation in mouse brain (Fifkova and van Harreveld, 1977). Also, transient axonal swelling, coincident with passage of the compound action potential has been observed in the non-myelinated garfish olfactory nerve *ex vivo* (Tasaki and Byrne, 1992). Thus neuronal cells may make some additional contribution to activity-dependent shrinkage of the extracellular space in white matter. Regardless of the precise cellular origins, ECS shrinkage would be expected to result in an overall reduction in tissue water diffusivity. Indeed, in mathematical modeling of diffusion in white matter, the extracellular volume fraction is shown to be a dominant factor in determining the overall tissue diffusion characteristics (Sen and Basser, 2005).

A number of neurological disorders originate with white-matter pathology. Hence, it is envisioned that diffusion fMRI may provide information complementary to that provided by structural/anatomical images and possibly a means to directly monitor the effects of disease progression or treatment response on white-matter function in this context. From the standpoint of basic investigations of distributed neural networks, white-matter diffusion fMRI may provide interesting information that is not directly available by BOLD studies of grey matter activation within these networks.

Acknowledgments

The authors thank Professors Joseph J.H. Ackerman and Marcus Raichle for valuable discussions. This work was supported in part by the Mallinckrodt Institute of Radiology; NIH R01NS047592, P01NS059560 and 5R01EB00208; and NMSS RG 4549A4/1

References

Adamczak JM, Farr TD, Seehafer JU, Kalthoff D, Hoehn M. High field BOLD response to forepaw stimulation in the mouse. Neuroimage. 2010; 51:704–712. [PubMed: 20211267]

Anderson AW, et al. Effects of osmotically driven cell volume changes on diffusion- weighted imaging of the rat optic nerve. Magn Reson Med. 1996; 35:162–167. [PubMed: 8622579]

Does MD, Zhong J, Gore JC. In Vivo measurement of ADC change due to intravascular susceptibility variation. Magn Reson Med. 1999; 41:236–240. [PubMed: 10080268]

Fifkova E, van Harreveld A. Long-lasting morphological changes in dendritic spines of dentate granular cells following stimulation of the entorhinal area. J Neurocytol. 1977; 6:211–230. [PubMed: 856951]

Garbow JR, McIntosh C, Conradi MS. Actively decoupled transmit-receive coil-pair for mouse brain MRI. Conc Magn Reson Pt B: Magn Reson Eng. 2008; 33B:252–259.

Gawryluk JR, Brewer KD, Beyea SD, D'Arcy RCN. Optimizing the detection of white matter fMRI using asymmetric spin echo spiral. NeuroImage. 2009; 45:83–88. [PubMed: 19084071]

Gulani V, Iwamoto GA, Lauterbur PC. Apparent Water Diffusion Measurements in Electrically Stimulated Neural Tissue. Magn Reson Med. 1999; 41:241–246. [PubMed: 10080269]

Hartline HK. Intensity and duration in the excitation of single photoreceptor units. J Cell Comp Physiol. 1934; 5:229–247.

Jones, DK., editor. Diffusion MRI: Theory, Methods, and Applications. 1. Oxford University Press; USA: 2010.

Latour LL, Hasegawa Y, Formato JE, Fisher M, Sotak CH. Spreading waves of decreased diffusion coefficient after cortical stimulation in the rat brain. Magn Reson Med. 1994; 32:189–198. [PubMed: 7968441]

Le Bihan D, Urayama S, Aso T, Hanakawa T, Fukuyama H. Direct and fast detection of neuronal activation in the human brain with diffusion MRI. Proc Natl Acad Sci, USA. 2006; 103:8263–8268. [PubMed: 16702549]

Lee K, Nawrot M, Garwin G, Saari J, Hurley J. Relationships among Visual Cycle Retinoids, Rhodopsin Phosphorylation, and Phototransduction in Mouse Eyes During Light and Dark Adaptation. Biochemistry. 2010; 49:2454–2463. [PubMed: 20155952]

Logothetis NK. What we can do and what we cannot do with fMRI. Nature. 2008; 453:869–878. [PubMed: 18548064]

Mandl RCW, Schnack HG, Zwiers MP, van der Schaaf A, Kahn RS, Pol HEH. Functional diffusion tensor imaging: measuring task-related anisotropy changes in the human brain along white matter tracts. PLoS One. 2008; 3:e3631. [PubMed: 18982065]

May CA, Lutjen-Drecoll E. Morphology of the murine optic nerve. Invest Ophthal Vis Sci. 2002; 43:2206–2212. [PubMed: 12091418]

Miller KL, Bulte DP, Devlin H, Robson MD, Wise RG, Woolrich MW, Jezzard P, Behrens TEJ. Evidence for a vascular contribution to diffusion fMRI at high b value. Proc Natl Acad Sci, USA. 2007; 104:20967–20972. [PubMed: 18093924]

Nakamura TJ, Ebihara S, Shinohara K. Reduced light response of neuronal firing activity in the suprachiasmatic nucleus and optic nerve of cryptochrome-deficient mice. PLoS One. 2011; 6:e28726. [PubMed: 22216107]

Prusky GT, Alam NM, Beekman S, Douglas RM. Rapid Quantification of Adult and Developing Mouse Spatial Vision Using a Virtual Optomotor System. Invest Ophthal Vis Sci. 2004; 45:4611–4616. [PubMed: 15557474]

Ransom BR, Sontheimer H. The neurophysiology of glial cells. J Clin Neurophys. 1992; 9:224–251.

Ransom BR, Yamate CL, Connors BW. Activity-dependent shrinkage of extracellular space in rat optic nerve: a developmental study. J Neurosci. 1985; 5:532–535. [PubMed: 3973681]

Rash JE. Molecular disruptions of the panglial syncytium block potassium siphoning and axonal saltatory conduction: pertinence to neuromyelitis optica and other demyelinating diseases of the central nervous system. Neuroscience. 2010; 168:982–1008. [PubMed: 19850107]

Ridder WH III, Nusinowitz S. The visual evoked potential in the mouse—Origins and response characteristics. Vision Res. 2006; 46:902–913. [PubMed: 16242750]

Rostrup E, Law I, Blinkenberg M, Larsson HBW, Born AP, Holm S, Paulson OB. Regional Differences in the CBF and BOLD Responses to Hypercapnia: A Combined PET and fMRI Study. NeuroImage. 2000; 11:87–97. [PubMed: 10679182]

Rothe T, Bahring R, Carroll P, Grantyn R. Repetitive firing deficits and reduced sodium current density in retinal ganglion cells developing in the absence of BDNF. J Neurobiol. 1999; 40:407–419. [PubMed: 10440740]

Schwartzkroin PA, Baraban SC, Hochman DW. Osmolarity, ionic flux, and changes in brain excitability. Epilepsy Res. 1998; 32:275–285. [PubMed: 9761327]

Sen PN, Basser PJ. A model for diffusion in white matter in the brain. Biophys J. 2005; 89:2927–2938. [PubMed: 16100258]

Sotak CH. New NMR measurements in epilepsy: diffusion-weighted magnetic resonance imaging of spreading depression. Adv Neurol. 1999; 79:925–929. [PubMed: 10514875]

Sykova E, Chvatal A. Extracellular ionic and volume changes: the role in glia-neuron interactions. J Chem Neuroanat. 1993; 6:247–260. [PubMed: 8104419]

Szabo K, Poepel A, Pohlmann-Eden B, Hirsch J, Back T, Sedlaczek O, Hennerici M, Gass A. Diffusion-weighted and perfusion MRI demonstrates parenchymal changes in complex partial status epilepticus. Brain. 2005; 128:1369–1376. [PubMed: 15743871]

Tasaki I, Byrne PM. Rapid structural changes in nerve fibers evoked by electric current pulses. Biochem Biophys Res Commun. 1992; 188:559–564. [PubMed: 1445300]

Tu TW, Budde MD, Quirk JD, Song SK. Using absorption-mode images to improve in vivo DTI quality. Proc Intl Soc Magn Reson Med. 2010; 18:4001.

Walz W. Role of glial cells in the regulation of the brain ion microenvironment. Prog Neurobiol. 1989; 33:309–333. [PubMed: 2479051]

Waxman, SG.; Bangalore, L.; Lazzarini, R.; Griffin, JW.; Lassman, H.; Nave, KA.; Miller, R.; Trapp, BD., editors. Myelin Biology and Disorders. Elsevier Academic Press; 2004.

Zhong J, Kennan RP, Gore JC. Effects of susceptibility variations on NMR measurements of diffusion. J Magn Reson. 1991; 95:267–280.

Zhong J, Petroff OAC, Pleban LA, Gore JC, Prichard JW. Reversible, reproducible reduction of brain water apparent diffusion coefficient by cortical electroshocks. Magn Reson Med. 1997; 37:1–6. [PubMed: 8978625]

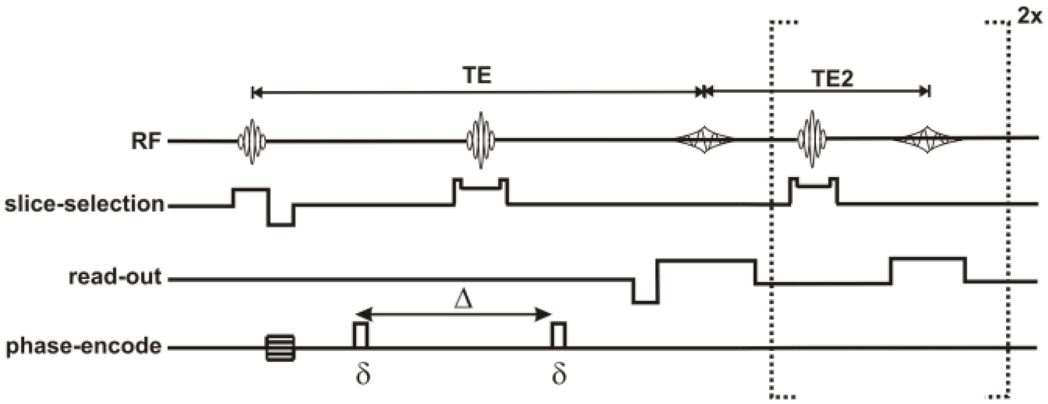

Figure 1.
Pulse sequence diagram for the diffusion-weighted multi-spin-echo sequence. Timing parameters include: δ = 5 ms, Δ = 18 ms, TE = 37.1 ms TE2 = 23.6 ms.

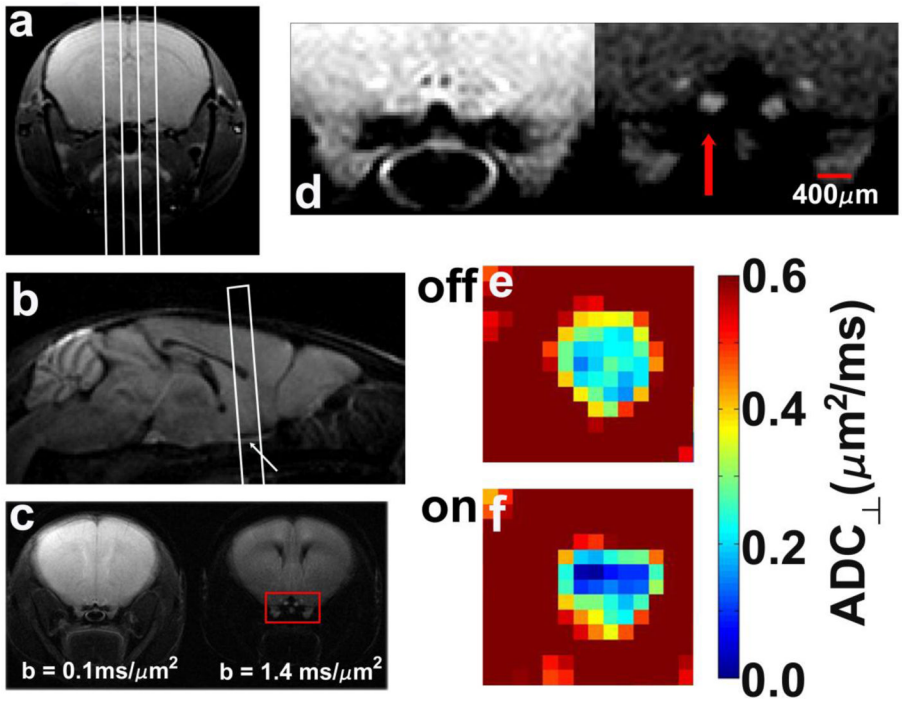

Figure 2.

Typical scout planning images **(a,b)**, final targeted images for diffusion measurements **(c,d)**, and $ADC_{\perp}$ maps of an optic nerve without **(e)** and with visual stimulation **(f). (a)** A multi-slice set of axial images of the mouse brain is acquired with a non-diffusion-weighted multi-echo spin-echo image (only a single slice is shown here) are used to plan sagittal slices, indicated by the white lines. **(b)** The center sagittal slice, acquired with diffusion-weighting gradients applied in the slice-select direction, captures both optic nerves (arrow) and is used to target the slice for measurements of $ADC_{\perp}$ and $ADC_{\parallel}$. **(c)** A pair of diffusion-weighted images with diffusion-sensitizing gradients applied in the phase-encode direction (left-to-right in the images). The optic nerve fibers are perpendicular to the slice plane in this final targeted slice. **(d)** Magnified view of the area within the red box of panel **c**. The left-hand image was acquired with b = 0.1 ms/μm^2, and the right-hand image with b = 1.4 ms/μm^2. Both optic nerves are clearly visible in the high-b image and the stimulated optic nerve indicated by the red arrow. Color maps of $ADC_{\perp}$ in an experimental optic nerve without **(e)** or with **(f)** visual stimulation.

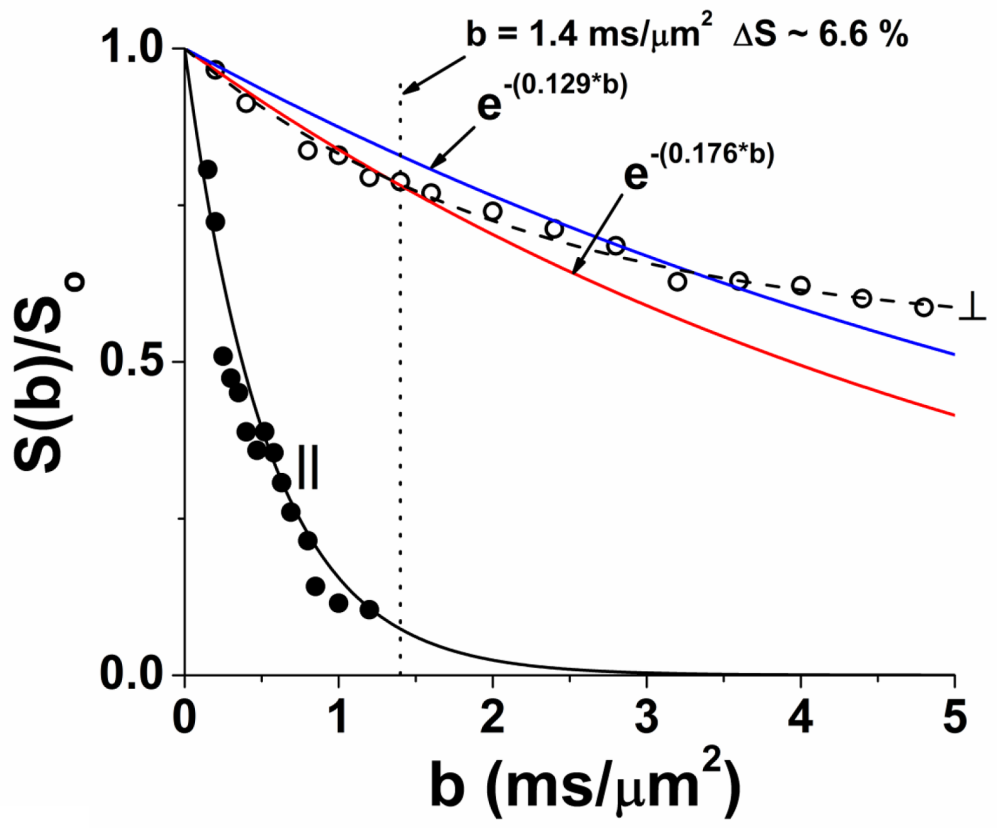

Figure 3.

Diffusion attenuation curves for a set of mouse optic nerves (n = 3) with diffusion weighting perpendicular and parallel to the nerve fibers (without visual stimulation), acquired with (δ = 5 ms, Δ = 18 ms). Parallel diffusivity is essentially mono-exponential. It is readily apparent that diffusion perpendicular to the fibers is highly restricted and non-monoexponential. The blue and red curves are constructed with $ADC_{\perp}$ = 0.129 μm^2/ms (blue curve, representative of activated optic nerve) and $ADC_{\perp}$ = 0.176 μm^2/ms (red curve, representative of unstimulated optic nerve). This figure is intended to emphasize that the large (27%) stimulus-induced decrease in $ADC_{\perp}$ results in a modest 6.6% signal increase at b = 1.4 ms/μm^2 with visual stimulation.

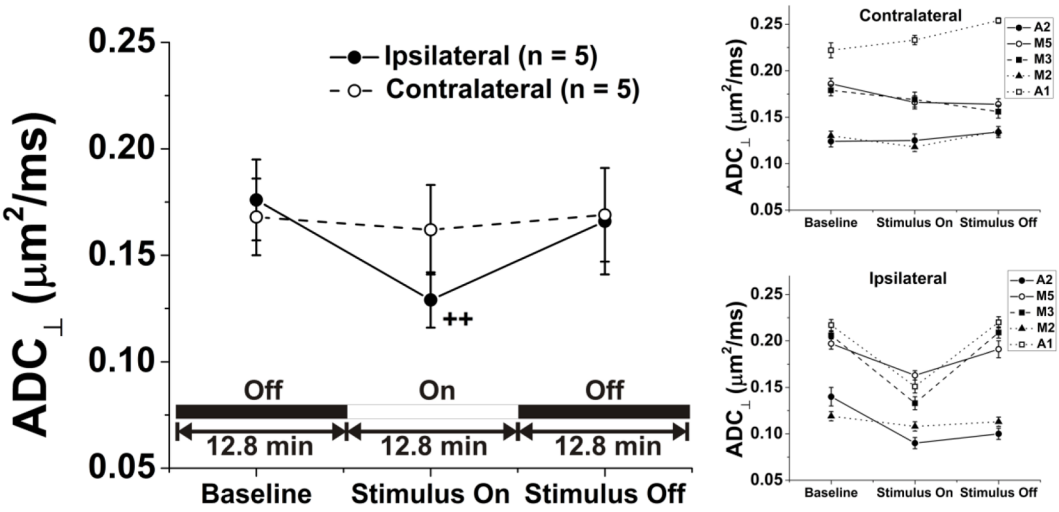

Figure 4.

Application of visual stimulus produces a significant drop in $ADC_{\perp}$ for the optic nerve of the stimulated eye [Baseline: 0.176 ± 0.019 μm^2/ms (mean ± sem), Stimulus On: 0.129 ± 0.013 μm^2/ms, ++: p = 0.0008], but no change for the contralateral, unstimulated eye. $ADC_{\perp}$ in the ipsilateral optic nerves returns to baseline values once again with removal of the stimulus. Quantities shown are the mean ± sem for image voxels within the optic nerve ROI in a group of five experimental mice breathing room air. The insets depict the measurements for the experimental/ipsilateral and control/contralateral optic nerves in individual animals.

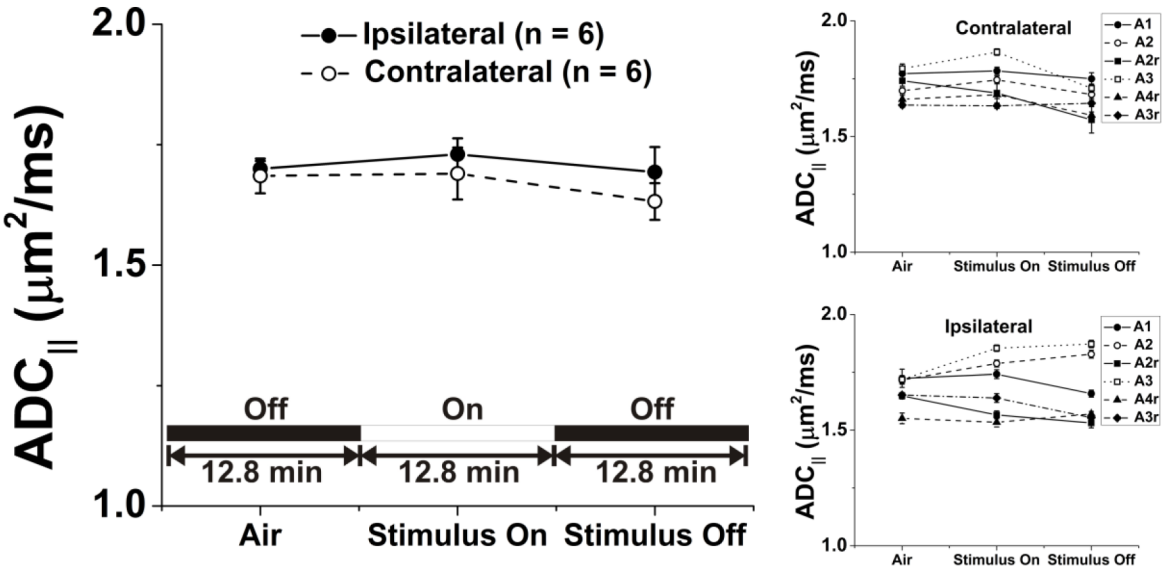

Figure 5.
Stimulus and $ADC_{||}$ in optic nerve of mice breathing room air. Quantities plotted are mean ± sem). Stimulation produces no statistically-significant changes in $ADC_{||}$.

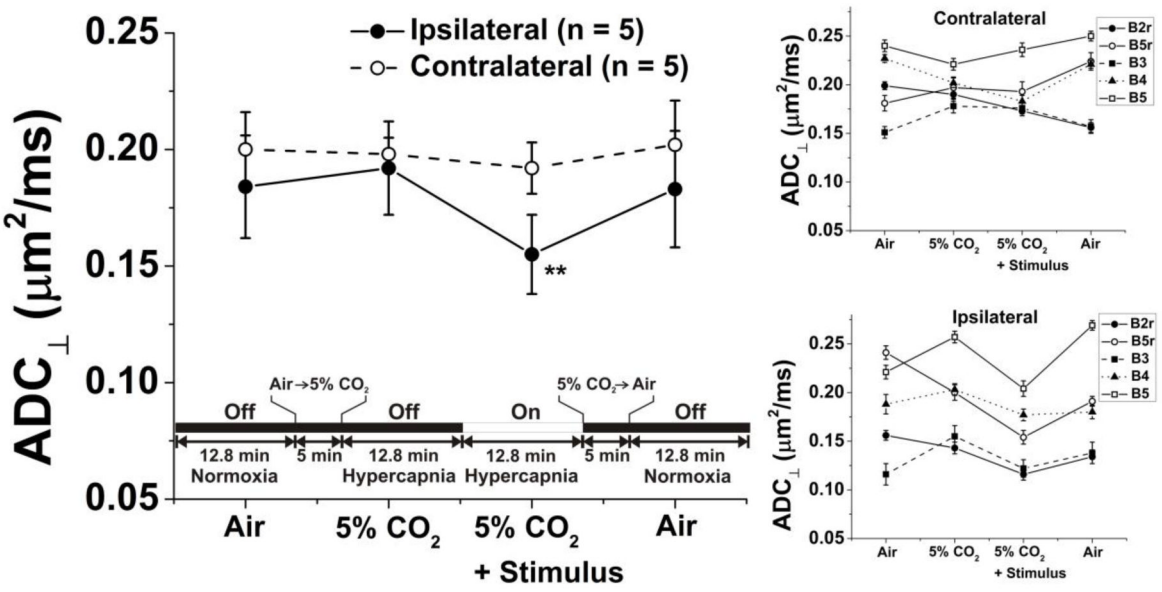

Figure 6.

The effects of hypercapnia on measured $ADC_{\perp}$ (mean ± sem) with and without stimulation were investigated in a set of mice in order to investigate vascular contributions to the observed phenomenon. The effects of stimulation on $ADC_{\perp}$ (a 19% decrease) was similar to changes seen in animals breathing room air.

Table 1

Measured $ADC_{\perp}$ (mean ± sem, n = 5) and $ADC_{||}$ (mean ± sem, n = 6) for *In Vivo* Mouse Optic Nerve in Room-Air-Breathing Mice.

Condition	Ipsilateral $ADC_{\perp}$ ($\mu m^2/ms$)	Contralateral $ADC_{\perp}$ ($\mu m^2/ms$)	Ipsilateral $ADC_{||}$ ($\mu m^2/ms$)	Contralateral $ADC_{||}$ ($\mu m^2/ms$)
Baseline	0.176 ± 0.019	0.168 ± 0.018[c]	1.70 ± 0.02	1.69 ± 0.04
Stimulus On	0.129 ± 0.013[a]	0.162 ± 0.021[d]	1.73 ± 0.03	1.69 ± 0.05
Stimulus Off	0.166 ± 0.025[b]	0.169 ± 0.022[e]	1.69 ± 0.03	1.63 ± 0.04

[a] p = 0.0008 vs. Ipsilateral “Baseline” group

[b] p = 0.005 vs. Ipsilateral “Stimulus On” group

[c] p = 0.004 vs. Ipsilateral “Stimulus On” group

[d] p = 0.01 vs. Ipsilateral “Stimulus On” group

[e] p = 0.003 vs. Ipsilateral “Stimulus On” group

Table 2

Measured $ADC_{\perp}$ (mean ± sem) for *In Vivo* Mouse Optic Nerve in Mice Breathing Air or 5% CO_2/95% O_2 (n = 5).

Condition	Ipsilateral $ADC_{\perp}$ (μm^2/ms)	Contralateral $ADC_{\perp}$ (μm^2/ms)
Air, Baseline	0.184 ± 0.022	0.200 ± 0.016[d]
5% CO_2, Baseline	0.192 ± 0.020	0.198 ± 0.007[e]
5% CO_2 + Stimulus	0.155 ± 0.017[a,b]	0.192 ± 0.011[f]
Air, Stimulus Off	0.183 ± 0.025[c]	0.202 ± 0.019[g]

[a] p = 0.03 vs. Ipsilateral “Air, Baseline” group

[b] p = 0.008 vs. Ipsilateral “5% CO_2, Baseline” group

[c] p = 0.04 vs. Ipsilateral “5% CO_2 + Stimulus” group

[d] p = 0.002 vs. Ipsilateral “5% CO_2 + Stimulus” group

[e] p = 0.002 vs. Ipsilateral “5% CO_2 + Stimulus” group

[f] p = 0.007 vs. Ipsilateral “5% CO_2 + Stimulus” group

[g] p = 0.001 vs. Ipsilateral “5% CO_2 + Stimulus” group